Molecular Catalysis 565 (2024) 114392

Contents lists available at ScienceDirect

Molecular Catalysis

journal homepage: www.journals.elsevier.com/molecular-catalysis

Iron, Cobalt and Nickel complexes with N4-donor ligands catalysts for the CO_2 photoreduction

Nassima El Aouni [a,b], Ali Aghmiz [b], Mar Reguero [a,*], Anna M. Masdeu-Bultó [a,*]

[a] Department of Physical and Inorganic Chemistry. Universitat Rovira i Virgili. Carrer Marcel·lí Domingo, 1. Campus Sescelades. 43007 Tarragona. Spain
[b] Equipe de Chimie Organique Appliquée à la Valorisation des Ressources Naturelles et Protection de l'Environnement, Laboratoire de Chimie et Microbiologie Appliquées et Biotechnologies, FS, Abdelmalek Essaadi University Tetouan, Morocco

ARTICLE INFO

Keywords:
Iron
Cobalt
Nickel
N4-donor ligands
Schiff base ligands
Carbon dioxide
DFT calculations

ABSTRACT

Iron(II), cobalt(II) and nickel (II) complexes bearing phenanthroline- and bipyridine-bis(imino) ligands have been prepared and tested as catalysts for the photoreduction of CO_2 at atmospheric pressure and room temperature in the presence of a photosensitizer (PS) and sacrificial electron donor (SD) producing mixtures of CO and H_2. The best results were obtained with a Fe(II) catalyst using triethanolamine/1,3-dimethyl-2-phenyl-2,3-dihydro-1H-benzoimida-zole (BIH) in acetonitrile using a blue LED irradiation with $[Ru(bpy)_3]PF_6]_2$ (bpy = 2,2′-bipyridine) as PS. With this system, a mixture of CO/H_2 (68/32) was obtained with a turnover number (TON_{CO} 166, 24 h). Analogous Co(II) and Ni(II) complexes produced H_2 as a major product. Cyclic voltammetry demonstrates that the electrons uptake is centered on the ligand. Computational calculations allow to propose the most stable location of the electrons.

1. Introduction

Anthropogenic emissions of carbon dioxide (CO_2) produced by the combustion of fossil fuels and industrial activity generate enormous quantities of this gas (estimated at 45 ± 5.5 Gt in 2019) [1]. The accumulation of CO_2, a greenhouse gas (GHG), in the atmosphere is causing major economic and human damage due to climate change [2]. To reduce these emissions, the CO_2 should be captured and at the same time, alternative non-fossil fuels should steadily replace oil. As the capture technologies are introduced, more CO_2 will be available and ready to be used as feedstock, but nowadays only a small part of the emissions is used as a chemical feedstock (<1 %) [3]. Using CO_2 as a starting material for oil derivatives may be a good alternative to reuse a waste, whose production is located in non-oil producers such as EU countries, but the cost of processing the CO_2 feedstocks (capture and transport) should be balanced by the profit obtained with its uses as such or with the chemicals obtained with its transformation [4]. Consequently, research on chemical processes for the transformation of CO_2 should be developed to reduce costs. Especially interesting is the conversion of CO_2 into chemicals [5,6] and fuels to close the carbon cycle [7]. Among the valuable products that can be obtained by the reduction of CO_2 are carbon monoxide (CO), formic acid (HCOOH), methanol (MeOH), and methane (CH_4) [8]. CO is used for many applications like carbonylation reactions leading to carboxylic acid derivatives or, combined with hydrogen (syn gas), it is used for the production of synthetic fuels, aldehydes, alcohols [9,10] or other chemicals using tandem reactions [11–13]. So obtention of CO or mixtures of CO/H_2 has an industrial interest.

Being CO_2 a highly stable molecule ($\Delta G_f^0 = -394.228$ kJ/mol) [14], its transformation requires a catalyst and high energy, which can be provided by electro-, photo- or photoelectrochemical methods. Photocatalysis is, probably, the most convenient method since it can use the energy provided continuously by the sun ($1.5{\cdot}10^5$ terawatts) which exceeds largely the energy used by human activities currently (ca 13 TW/h) [15]. Nevertheless, the efficiency of the photocatalysts is, in general, low, and research in this area is still necessary. The catalysts used for this process should fulfil the requirements of being active, selective, and with the highest availability and the lowest possible price. Catalytic systems consist of a catalyst, which may be a semiconductor or a molecular coordination compound, a light harvester, and a sacrificial electron donor. Highly active catalytic materials are hybrid combinations of photoactive semi-conductors with molecular complexes acting as catalysts [16–20]. The molecular catalysts introduce the possibility of easily modifying the active metal center properties through the ligands

* Corresponding authors.
E-mail addresses: mar.reguero@urv.cat (M. Reguero), annamaria.masdeu@urv.cat (A.M. Masdeu-Bultó).

https://doi.org/10.1016/j.mcat.2024.114392
Received 15 June 2024; Received in revised form 13 July 2024; Accepted 13 July 2024
Available online 19 July 2024

designed to achieve better results [21]. So, the development of molecular catalysts is important to reach high activities and selectivities to make the CO_2 transformation useful.

Molecular catalysts based on earth-abundant metal complexes such as iron, cobalt, and nickel stand out as the most desired candidates due to their availability, low cost, and low toxicity [22]. Ligands based on porphyrin [23,24], pyridyl [25–32], and cyclam (1,4,8,11-tetraazacyclotetradecane) [33,34] skeletons have proved to be the most suitable to participate as electron reservoirs and stabilizers of the low valent metal species involved in the CO_2 activation. Especially, bipyridine Re(I) based catalysts were reported by Lehn's group to be selective in the CO_2 photoreduction to CO [35,36] in the early 80 s. Most recently, Fe(II) and Co(II) polypyridyl-based systems in the presence of $[Ru(bpy)_3][PF_6]_2$ (bpy= 2,2′-bipyridine) as a photosensitizer and a sacrificial donor such as triethanolamine (TEOA), triethylamine (TEA), or 1,3-dimethyl-2--phenyl-2,3-dihydro-1H-benzoimidazole (BIH) have been shown to be also efficient electron donors for this reaction [25–27]. The electrochemical and computational studies of iron bipyridine-bis(imine) complexes have shown the cooperativity of the ligand redox properties with the metal centre for the redox transformations [37]. Redox-active ligands facilitate multielectron reactions with non-noble metals in catalytic processes by stabilising high reactive intermediates [38]. Moreover, a combination of the redox properties and structural parameters of the ligands may modify the participation of the metal centre in the catalytic electroreduction of CO_2 allowing changes in the selectivity of the products obtained [39,40] or even being the redox-active ligands responsible for the CO_2 reduction [41].

Based on the previously reported studies, we decided to focus our research for catalytic CO_2 photoreduction on a series of metal complexes with phenanthroline- and bipyridine-bis(imine) based ligands **1**–**3** (Scheme 1) with non-innocent ligands containing extensive conjugate π-systems to facilitate the electron acceptor and transfer processes. Different substituents on the aniline moieties (isopropyl and ethyl) were tried since their steric effects may affect the stability of the complex against hydrolisis of the imine and also the coordination number leaving empty coordination sites. We report here the synthesis of several series of complexes modifying different factors of their structure to analyze the impact of these changes on their catalytic activity in the photoreduction of CO_2 under mild conditions. We also developed a computational study to elucidate the more stable structures of some representative catalysts and their reduced species.

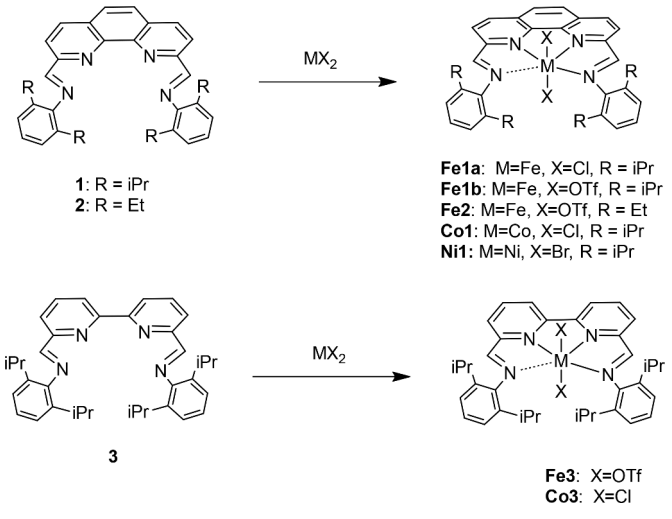

Scheme 1. Ligands and complexes used in this study (OTf = CF_3SO_3-).

2. Experimental section

2.1. Synthesis of complexes

2.1.1. Synthesis of bis(1,1′-(1,10-phenanthroline-2,9-diyl)bis(N-(2,6-diisopropylphenyl)-methanimine))bis(triflato)iron(II) (Fe1b)

A solution of $Fe(OTf)_2$ (0.088 g, 0.24 mmol) in acetonitrile (1.5 mL) was added to a solution of **1** (0.13 g, 0.25 mmol) in acetonitrile (1.5 mL). The mixture was stirred at room temperature for 18 h. After this time, it was filtered through celite and diethyl ether (10 mL) and hexane (0.5 mL) were added. The mixture was kept at −30 °C overnight. The product formed was filtered and washed three times with anhydrous hexane and vacuum dried to obtain a dark green product (0.077 g, 42 % yield).

Anal. Calcd. for $C_{40}H_{42}F_6FeN_4O_6S_2{\cdot}H_2O$ (926.8): C 51.8, H 4.8, N 6.1; found C 50.1, H 4.9, N 5.8. HRMS (ESI-TOF) *m/z* Calcd. for $C_{39}H_{42}F_3FeN_4O_3S$: 759.2279 [M-OTf], found: 759.2259. FTIR (cm^{-1}) (ATR): 3398 (w), 2963 (w), 2927 (w), 2869 (w), 1637 (w, C = N) 1616 (m), 1509 (m), 1536(m) 1463(m), 1442(w) 1385(w), 1363 (w), 1308 (m), 1281(m), 1252(m), 1232 (s) 1213 (s), 1160 (s), 1024 (s), 864 (m), 806 (m), 762 (m), 634 (s), 572 (m), 516 (m). Conductivity at $T = 25.0$ °C (CH_2Cl_2, 0.4 10^{-3} M): 15.7 S·cm^2/mol; (MeCN, 3.3·10^{-4} M): 191.9 S·cm^2/mol. UV–Vis (MeCN, 0.4 10^{-3} M): 250.0 nm (ε 1800 L.cm.mol^{-1}), 299.0 (ε 1388 L.cm.mol^{-1}). Molar magnetic susceptibility (Mohr balance) $\chi_M = 8.5.10^{-3}$ emu/mol, $\mu = 4.24\ \mu_B$.

2.1.2. Synthesis of (1,1′-(1,10-phenanthroline-2,9-diyl)bis(N-(2,6-diethylylphenyl)-methanimine))bis(triflato)iron(II) (Fe2)

A solution of $Fe(OTf)_2$ (0.088 g, 0.24 mmol) in acetonitrile (3 mL) was added to a solution of **2** (0.12 g, 0.25 mmol) in acetonitrile (2.5 mL). The mixture was stirred at room temperature for 18 h. After this time, it was filtered through celite and diethyl ether (20 mL) was added. The mixture was kept at −30 °C overnight. The product formed was filtered and washed three times with anhydrous hexane and vacuum dried to obtain a dark green product (0.1 g, 45 % yield).

Anal. Calcd. for $C_{36}H_{34}F_6FeN_4O_6S_2{\cdot}CH_3CN$ (893.7): C 51.1, H 4.2, N 7.8; found C 51.1, H 4.5, N 7.5. HRMS (ESI-TOF) *m/z* Calcd. for $C_{35}H_{34}F_3FeN_4O_3S$: 703.1653 [M-OTf], $C_{68}H_{68}Cl_2N_8Fe$ 526.2458 [Fe(**2**)$_2$]$^{2+}$, found: 526.2454. FTIR (cm^{-1}) (ATR): 3109 (s), 2965 (s), 2879 (w), 1731(m), 1710(m) 1634 (m, C = N) 1619 (m), 1606(m) 1558 (w), 1536 (w), 1508 (m), 1536(m) 1448(m), 1388(w), 1358 (m)1301(w), 1259(s) 1045 (vs) 1029 (vs) 866 (vs), 805 (s), 758 (s), 634 (s). Molar conductivity (MeCN, 3.52·10^{-4} M): 157.3 S·cm^2/mol a T = 25 °C. UV–Vis (MeCN, 0.26 10^{-3} M): 249.6 nm (ε 1351 L.cm.mol^{-1}), 299.0 (ε 1885 L.cm.mol^{-1}). Molar magnetic susceptibility (Mohr balance) χ_M = 9.97.10^{-3} emu/mol, $\mu = 4.84\ \mu_B$

2.1.3. Synthesis of 1,1′-([2,2′-bipyridine]−6,6′-diyl)bis(N-(2,6-diisopropylphenyl)-methanimine)bis(triflato)iron(II) (Fe3)

A solution of $Fe(OTf)_2$ (0.0637 g, 0.18 mmol) in 3 mL of acetonitrile was added dropwise for 15 min to a solution of **3** (0.10 g, 0.19 mmol) in 5 mL of acetonitrile. The mixture was stirred at room temperature for 18 h. After this time, it was filtered through celite and diethyl ether (10 mL) was added. The mixture was kept at −30 °C overnight. The product formed is filtered and washed three times with cold diethyl ether and vacuum dried to obtain a dark green product (0.08 g, 50 % yield).

Anal. Calcd. for $C_{38}H_{42}F_6FeN_4O_6S_2{\cdot}3H_2O$ (938.8): C 48.7, H 5.1, N 6.0; found C 47.2, H 4.8, N 5.9. HRMS (ESI-TOF) *m/z* Calcd. for $C_{38}H_{42}F_6FeN_4O_6S_2$: 735.2273 [M-OTf]$^+$, found: 735.2278 (100%). FTIR (cm^{-1}) (ATR) 3399 (w), 2966 (w), 2871 (w), 1629 (w, C = N) 1596 (m), 1524(m) 1464(m), 1437(m) 1386(w), 1365 (w), 1277(s), 1245(s), 1224 (s), 1166(s), 1026 (s), 797 (m), 633 (s), 573(m), 514(m). Conductivity (MeCN, 4.36 10^{-5} mol/L): 123.2 S·cm^2/mol a T = 23.5 °C. UV–Vis (MeCN, 4.36 10^{-5} mol/L): 291.0 nm (ε 7828 L.cm.mol^{-1}), 324 (ε 4702 L.cm.mol^{-1}). Molar magnetic susceptibility $\chi_M = 1.263.10^{-2}$ emu/mol, μ =5.46 μ_B

2.1.4. Synthesis of 1,1′-([2,2′-bipyridine]−6,6′-diyl)bis(N-(2,6-diisopropylphenyl)metha-nimine)bis(chlorido)cobalt(II) (**Co3**)

In a round bottom flask $CoCl_2$ (0.0899 g, 0.378 mmol) was mixed with n-butanol (10 mL) and was stirred at 100 °C till its dissolution. Then **3** (0.1 g, 0.189 mmol) was added to the mixture and it was stirred for 18 h under reflux. A green mixture was obtained, which was evaporated, and hexane was added to induce the precipitation. The solid was filtered off and washed with hexane to yield the product as a green powder (0.082 g, 66 % yield).

Anal. Calcd. for $C_{36}H_{42}Cl_2CoN_4{\cdot}3H_2O$ (759.6): C 56.9, H 6.0, N 7.4; found C 57.7, H 5.9, N 7.0. HRMS (ESI-TOF) *m/z* Calcd. for $C_{36}H_{42}ClCoN_4$: 624.2430 $[M\text{-}Cl]^+$, found: 624.2424 (100%). FTIR(cm^{-1}) (ATR) 3425 (w), 2959 (m), 2868 (w), 1632 (w, C = N) 1593 (m), 1463 (m), 1435(m) 1383(w), 1362 (w), 1327(w), 1171(s), 1100 (m), 1028 (m), 799 (s), 767 (m) 738 (m), 646 (w). Conductivity (MeCN, 7.11 10^{-5} mol/L): 24.6 S·cm^2/mol a $T = 25$ °C. UV–Vis (MeCN, 3.4 10^{-4} M): 207.0 nm (ε 7772 L.cm.mol^{-1}), 277.0 nm (ε 1980 L.cm.mol^{-1}), 323 (ε 1495 L.cm.mol^{-1}). Molar magnetic susceptibility $\chi_M = 1.36.10^{-3}$ emu/mol, μ = 1.79 μ_B.

2.2. Electrochemical experiments

Cyclic voltammetry (CV) measurements were performed with a Metrohm Autolab PGSTAT 204 potentiostat equipped with a 3 mm diameter glassy carbon polished and dried before use, Pt wire as a working electrode and Ag/AgCl (3 M KCl) as a reference electrode. The supporting electrolytes tetrabutylammonium hexafluorophosphate (≥99 %, Aldrich) 0.1 M in acetonitrile were used as received. In the experiments carried out under nitrogen, the solution was priory degassed by bubbling nitrogen and the CV experiments were run under a nitrogen atmosphere (flushing gently over the solution). In the experiments under carbon dioxide, the solution was bubbled with CO_2 for 20 min and the CV were run under gently flushing over the solution at room temperature in an electrolytic cell in a 25 mL solution. The potentials were adjusted to values of an external reference ferrocene/ferrocenium in acetonitrile (0.5 M) except otherwise indicated (Values vs Fc^+/Fc = $\varepsilon_{Ag/AgCl}$ - 0.421 V).

2.3. Computational methods

To determine the structure of the non-reduced and reduced species of the catalysts analysed computational tools were used. Minimum energy structures were found for all the species of interest, taking into account the possible isomers and multiplicities. Gibbs free energies (G) and frequencies (that confirmed that the structures found were energy minima) were also calculated.

All calculations performed in this study (geometry optimizations and frequency calculations) were carried out using the DFT method as implemented in Gaussian 16 [42]. Cam-B3LYP functional with Grimme's D3BJ empirical dispersion correction was used due to its good performance in similar systems. The basis set 6–311+*G*(2df,p) was used for all elements except for Fe, for which a LanL2DZ pseudopotential was used instead. To take into account the effect of the solvent, the Polarizable Continuum Model (PCM) was used [43].

Nevertheless, for the study of the reduced species, to improve the quality of the results, the PBE functional was used instead, with a basis set Aug-cc-DVTZ for all elements except for Fe, for which a LanL2TZ(f) pseudopotential was used.

The results of a previous exploratory work of our group [44], developed to corroborate the spin multiplicity of the lowest-energy Fe complexes of interest, have also been considered in this study and will be shown briefly in the results section. These simpler computations were performed in vacuum with the M06 functional, using a 6–31G** for all elements except for Fe, for which a LanL2DZ pseudopotential was used.

In the study of the possible substitution of triflate ligands by acetonitrile molecules, to compare energies of the different possible complexes formed, the systems were considered to be formed by {[Fe(**1**)$(OTf)_n(MeCN)_{2\text{-}n}]^{2\text{-}n}$ + (2-n) OTf^- + *n* MeCN} for *n* = 0–2, keeping always in this way the same number of particles. The large difference in the concentrations of the triflate and MeCN free ligands, though (14.81 M for MeCN v.s. 0.0004 M for each triflate dissociated), made it advisable to include in the calculation of the free energies (G) the correction to the entropic term due to the deviation from the standard concentration.

2.4. Catalysis

2.4.1. Photocatalytic experiments

In a typical experiment, a 12 mL vial was filled with a mixture containing the catalyst ($4{\cdot}10^{-4}$ M) and the photosensitizer ($1.66{\cdot}10^{-3}$ M) dissolved in mixtures of TEOA with N-methyl-2-pyrrolidone (NMP) or acetonitrile (MeCN) (1/5 v/v) to a total liquid volume of 3.5 mL (8.5 mL free headspace gas volume) under nitrogen. The solution was saturated with CO_2 by bubbling slowly for 20 min to avoid solvent evaporation. The vial was placed at 11 cm from two blue LED Kessil lights sources positioned on both opposite sides of the sample (λ= 456 nm, max 50 W; and 467 nm, max 44 W) and kept under stirring refrigerated with a fan. The% CO and% H_2 concentrations were analyzed by a gas chromatograph equipped with a thermal conductivity detector (GC-TCD, Agilent 7890A) equipped with a capillary column HP-PLOT 5A calibrated with premixed CO/N_2 and H_2/N_2 mixtures. Manual injections (100 μL) were made with a gastight syringe (Hamilton). The moles of gases were calculated considering 8.5 mL as the headspace volume and the ideal gas law ($R = 0.082$ at l K^{-1} mol^{-1}; $T = 298$ K; $P = 1$ atm). The experiments were done in duplicate or repeated until consistent results (up to 8 % deviation from averaged data). An example of a chromatogram is shown in Figure S2 (Supplementary information).

2.4.2. Formic acid analysis

Formic acid content was analysed by high-performance liquid chromatography (HPLC) following a previously reported procedure after extraction from the sample [45,46]. A volume of 1 mL of miliQ water was added to 1 mL of the crude. Sulfuric acid (0.22 mL 1.0 M in miliQ water) was added to achieve 10 % v/v of the resulting solution. The solution was extracted with ethyl acetate (2.25 mL). The upper organic layer (10 μL) was injected into a 1200 Series HPLC equipped with a Diode Array Detector G1315D using a Rezex TM ROA-Organic Acid *H*+ column 300 × 7.8 mm (Phenomenex) and 5 mM H_2SO_4 (0.5 ml/min) as the mobile phase in isocratic mode from the *Serveis Científico Tècnics* (University Rovira i Virgili).

3. Results and discussion

3.1. Synthesis of ligands and complexes

The syntheses of ligands **1**–**3** (Scheme 1) were previously reported [47–49]. The complexes [Fe(**1**–**3**)$(OTf)_2$] (**Fe1b-3**, OTf = -O_3SCF_3) were prepared by reaction of the $Fe(OTf)_2$ with the corresponding ligand. They were obtained as dark green solids with moderate to good yields (42–60 %). The mass spectrometry ESI-TOF and elemental analysis agree with the [Fe(**1**–**3**)$(OTf)_2$] formulation. FT-IR shows the presence of the stretching vibration (ν) of the imine (ca 1635 cm^{-1}) and the aromatic amine frequencies (ca 1620 cm^{-1}). The value of conductivity in dichloromethane of **Fe1b** indicates that the triflate anions are coordinated (15 S·cm^2/mol) [50], although in a coordinating solvent such as acetonitrile the value of conductivity (191.9 S·cm^2/mol) agrees with the dissociation of the two triflate ligands (Λ_M values close to the range of 220–300 S.cm^2. mol^{-1} considered for 1:2 electrolytes). The lower values of molar conductivity Λ_M obtained for **Fe2** and **Fe3** (157.3 S·cm^2/mol and 123.2 S.cm^2. mol^{-1} respectively) may indicate that only one triflate is substituted [50]. In contrast, the conductivity value in an acetonitrile solution of **Co3** indicates that the chloride does not dissociate $\Lambda_M = 24.6$

S.cm^2. mol^{-1}). The magnetism at room temperature of the iron complexes (values of magnetic moment μ 4.2–5.5 μ_B) points to high spin systems as reported for similar complexes [51]. Complex **Co3** was prepared by a similar procedure as its analogous **Co1** [52] and presented a value of magnetic moment (1.99 μ_B) compatible with a low spin situation ($S = 1/2$).

The geometry of the complexes depends on the denticity of the **1–3** ligands. In the literature we can find phenanthroline- and bipyridine-(bis)imine ligands acting as tetra- or tridentate ligands. For example, the X-ray diffraction structure of a related system with a mesitylene group showed an octahedral geometry with the ligand acting as tetradentate [37]. So were the reported complexes of Fe(II) and Ni(II) with phenanthroline bis(benzothiazolate) derivative ligands [53]. Instead, according to the literature, the chloride analogous of **Fe3** with a mesitylene group presents a five-coordinate iron centre with the ligand acting as tridentate. It was observed a π-π stacking between the bipyridyl fragments and the mesityl ring of the not coordinated ligand arm facilitated by the larger flexibility of the bipyridil skeleton; resulting overall in a five-coordinate metallic center [51]. Ni(II) and Co(II) halide complexes with **1,** which bears voluminous isopropyl groups, were reported also to have a pentacoordinate environment according to the X-ray diffraction structures reported [52]. Furthermore, homoleptic systems have been also reported in which the octahedral coordination geometry is occupied by two tridentate ligands, in the case of ligands presenting only one thioether group in the aromatic ring [54]. In the absence of X-ray diffraction data for complexes **Fe1b-3**, we decided to use density functional theory (DFT) calculations to determine which geometries were the most stable ones. Previous computational studies of the relative stability of Zn(II) complexes with these ligands have demonstrated that this is a good tool to predict the structures of this kind of systems [49].

3.2. Electronic configurations and geometry structures determined computationally

The computational study had to determine, first, the electronic structure of the Fe complexes. In a previous study developed in the group [44], DFT calculations (computational conditions described in Experimental Section) for the derivatives of the **Fe1a** complex such as **Fe1aH** (Fig. 1) and **Fe1aEt** (Fig. 1) were carried out to determine the most stable spin configuration. High spin (HS, with $S = 2$, quintuplet multiplicity), intermediate spin (IS, with $S = 1$, triplet multiplicity) and low spin (LS, with $S = 0$, singlet multiplicity) were considered. We also took into account the possible hexa-, penta- and tetracoordinate isomers, obtained as a result of the possible *endo* or *exo* orientation of the imino groups (located outside the coordination sphere), that determine if the metal centre can coordinate with 2, 3 or 4 of the N atoms of the ligand. These results, collected in Fig. 1 and Table S1 of the Supporting Information, showed that in all cases the HS electronic configuration was the most stable one. This agrees with our experimental observations (vide infra) and with previous reports for similar Fe(II) complexes [51].

We also found that in all cases the hexa-coordinated species was the most stable one (except in the case of **Fe1aH**, where the penta-coordinated one was slightly more stable), but the energy difference between species with different coordination number (CN) were small (less that 1 kcal/mol in many cases). For this reason, a more detailed study has been performed here, considering the complex in acetonitrile solution.

For this new study, developed for the **Fe1aH, Fe1a** and **Fe1b** complexes, the computational conditions have been the ones described in Experimental Section (Cam-B3LYP + dispersion correction; basis set: 6–311+*G*(2df,p)+LanL2DZ (Fe,Cl,S); solvent model: PCM). Here, apart from the *endo/exo* conformation of the imine groups, we also considered *cis/trans* isomers of the imine double bond when sterical interactions allowed it, as well as possible disrotatory/conrotatory orientations of the planes of the two aryl moieties (when the aromatic rings were not parallel), although not in all cases stable structures were found. The relative energies of the stable isomers found are displayed in Table 1, and some representative geometries are shown in Figure S1 of Supporting Information.

In all cases, the hexacoordinated species proved to be the most stable one. The free-energy difference with the second more stable species, the pentacoordinate one, corresponds to a presence of this last isomer of 2.6 % for **Fe1aH**, 0.3 % for **Fe1a** and 10^{-5} % for **Fe1b**, what shows that it can

Table 1
Free energies (relative to the hexacoordinated structure) of isomers of complexes **Fe1H, Fe1a** and **Fe1b** calculated at Cam-B3LYP level.

Fe1aH		ΔG (kcal mol^{-1})
6-coord.	*endo-trans/endo-trans*	0
5-coord.	*endo-trans/exo-trans*	2.2
	endo-trans/exo-cis	8.6
4-coord.	*exo-trans/exo-trans*	11.8
	exo-trans/exo-cis	17.1
	exo-cis/exo-cis	20.3
G_{ref} = −1373.2032 a.u.		
Fe1a		ΔG (kcal mol^{-1})
6-coord.	*endo-trans/endo-trans*	0.0
5-coord.	*endo-trans/exo-trans*	3.4
4-coord. disrot	*exo-trans/exo-trans*	10.5
4-coord. conrot	*exo-trans/exo-trans*	11.9
G_{ref} = −1844.4222 a.u.		
Fe1b		ΔG (kcal mol^{-1})
6-coord.	*endo-trans/endo-trans*	0.0
5-coord.	*endo-trans/exo-trans*	8.8
4-coord	*exo-trans/exo-trans*	20.3
G_{ref} = −2960.6529 a.u.		

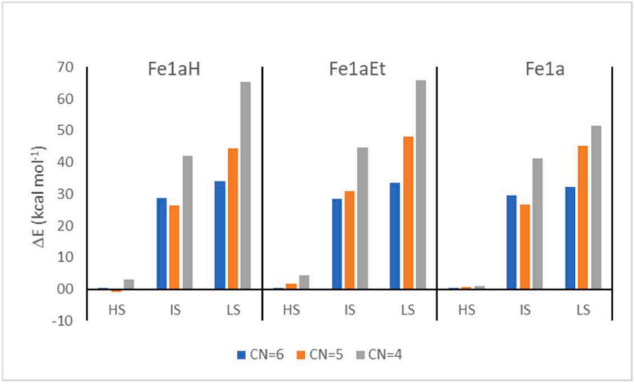

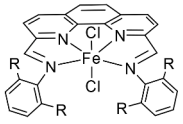

Fe1aH: R = H
Fe1aEt: R = Et

Fig. 1. Energies (relative to the HS species of the 6-coordinated isomer) of the possible spin states for the different isomers (with coordination 6, 5 and 4) of the complexes **Fe1aH, Fe1aEt** and **Fe1a**. Previous results of the group (data in Table S1) [44].

be considered that only the hexacoordinated structure of the complex is present in solution.

Nevertheless, in the case of compound **Fe1b**, given that in an acetonitrile solution, the triflate ligands could be substituted by solvent molecules, we studied explicitly these possible substitutions. In fact, taking into account the lability of the triflate ligand, we considered also some penta-coordinated species. Following the strategy described in the Computational methods section, we obtained the results collected in Table 2 (more detailed numerical results are shown in Table S2 of Supporting Information).

These results indicate that the substitutions considered are favourable and the most stable species is the hexacoordinate complex [Fe(**1**)$(MeCN)_2]^{+2}$, in agreement with measurements of conductivity that indicate that one or two triflate ligands dissociate. Nevertheless, the small energy difference with the monosubstituted species (less than 1 kcal mol^{-1}), indicates that a significant 38 % of this species could exist in solution, while only 2 % of the species in solution would correspond to the most unstable non-substituted complex containing two triflate ligands (ΔG = 2.3 kcal mol^{-1}). The pentacoordinate species, much less stable, are predicted not to be present.

3.3. Photocatalytic reduction of CO_2

The catalytic activity of the Fe, Co and Ni complexes with ligands **1–3** in the photocatalytic reduction of CO_2 was studied using irradiation of a blue LED light (λ = 456 nm and 467 nm) in the presence of the photosensitizer $[Ru(bpy)_3][PF_6]_2$ (**PS1**), and a sacrificial electron donor (SD). Also, the catalytic activity of the related complex **Zn1** (Zn(**1**)Cl_2) previously reported was included as a reference [49]. The gas composition (CO and H_2) of the catalytic tests was analyzed by gas chromatography with a thermal conductivity detector (GC-TCD). The possible content of formic acid of the catalytic solution was analyzed by HPLC after derivatization but no HCOOH was detected in any case. The initial screening was performed under previously reported conditions using triethanolamine (TEOA) as SD and N-methyl-2-pyrrolidone (NMP) as solvent [25]. NMP has demonstrated good absorption of CO_2 in the Purisol® capture process [55]. The initial blank test using only the PS produced a very small amount of CO and H_2 (entry 1, Table 3), so, in this case, the possible CO and H_2 products generated by the photolysis of the reaction medium can be neglected [56]. In the absence of the PS, neither CO nor H_2 was detected (entry 2, Table 3). A screening to determine the influence of the metal centre showed that, under these conditions, iron catalyst **Fe1a**, produced mixtures ca 1:1 of CO/H_2 during the first 4 h (entry 3, Table 3) but the H_2 production increased after 24 h (entry 4, Table 3). Instead, the cobalt and nickel catalysts, **Co1** and **Ni1**, formed H_2 as the main product (86–100 %, entries 5–7, Table 3). In the case of cobalt catalysts, the formation of H_2 was explained in the literature [54] by the reaction of cobalt-hydride species $[Co^{III}L(H)]^{2+}$ with H^+, where these Co^{III}-H species may be formed by the reaction of Co^{II} or Co^{I} complexes with H^+ donors (TEOA or traces of H_2O) present in the reaction media [34]. Then, in our case, the formation of H_2 as the major product may be related to the unfavored formation of Co^{I} species to react with CO_2 or to the fact that the formation of Co^{I}-CO_2 adduct is slow [34,57]. Mononuclear Ni-cyclam complexes reported in the literature produced mixtures with H_2 as the main product (CO/H_2 ratios 0.4–0.1) under photocatalytic conditions (**PS1** and aqueous system) [58,59].

Table 2
Free energies relative to the most stable species ($[Fe(\mathbf{1})(MeCN)_2]^{+2}$, multiplicity= 5) of possible species derived from the original complex by substitution of 1 or 2 triflate ligands by 2 or 1 MeCN solvent molecules and by dissociation of one of those ligands (different possible multiplicities considered in these last cases).

Species	CN	Multiplicity	ΔG (kcal/mol)
$[Fe(1)(OTf)_2]$	6	5	2.3
$[Fe(1)(OTf)(MeCN)]^+$	6	5	0.6
$[Fe(1)(MeCN)_2]^{+2}$	6	5	0.0
$[Fe(1)(OTf)_1]^+$	5	5	6.7
		3	29.0
		1	41.9
$[Fe(1)(MeCN)_1]^{+2}$	5	5	7.7
		3	30.6
		1	39.0

Table 3
Effect of the catalyst in the photoreduction of CO_2[a].

Run	Catalyst	Solvent/ SD	CO (μmol)	TON_{CO} (% Sel)	H_2 (μmol)	TON_{H2} (% Sel)
1	–	NMP	1.6	0.2[b]	7.7	0.8[b]
2[c]	Fe1a	NMP	0	0	0	0
3[d]	Fe1a	NMP	7.8	6 (48)	8.4	6 (52)
4	Fe1a	NMP	7.4	5 (31)	16.4	12 (68)
5[d]	Co1	NMP	8.9	6 (15)	51.6	34 (85)
6	Co1	NMP	8.2	5 (14)	49.1	33 (86)
7	Ni1	NMP	0	0 (0)	40.5	27 (100)
8	Fe1b	NMP	11.7	8 (35)	21.3	14 (65)
9	Fe1b	MeCN	0	–	0	–
10[d]	Fe1b	MeCN	25.1	17 (29)	93.4	62 (79)
11	Fe2	MeCN	19.3	13 (24)	59.6	40 (75)
12[e]	Fe3	MeCN	21.0	14 (36)	38.0	26 (64)
13	Co3	MeCN	11.1	8 (6)	167.6	112 (94)
14	Zn1	MeCN	1.4	0.9 (19)	6.0	4 (81)

[a] Reaction conditions: Catalyst 0.4 mM; TEOA/solvent: 1/5 v/v; NMP = *N*-methylpyrrolidone, MeCN= acetonitrile. PS = $[Ru(bpy)_3]PF_6]_2$ (1.66 mM), time 24 h. Light source: blue LED (λ = 456, 467 nm). TON = turn over number calculated as mols of product/mol catalyst. [b] Respect to Ru. [c] No PS. [d] Reaction run under N_2. [e] Time = 4 h.

Using the catalyst **Fe1b**, containing a less coordinating ion such as triflate, led to a slightly more active system (entry 8, Table 3). A blank experiment run under the same catalytic system under N_2 did not produce gas products, confirming that CO_2 is necessary to produce CO (entry 9, Table 3). Furthermore, when NMP was replaced by MeCN (1/5 v/v) a two-fold increase of the activity was observed (entry 10, Table 3). Although the solubility of CO_2 in saturated MeCN was estimated to be 0.38 M [60], similar to the values reported for NMP [61] and both solvents have coordination ability and may replace the triflate ligands [62], NMP may lead to more stable intermediate species less reactive.

Regarding the steric effect of the ligand, when the ethyl derivative **Fe2** was used as a catalyst, slightly lower activity and selectivity were obtained than using the isopropyl derivative (entry 11, Table 3). An effect of the skeleton was also observed when the catalyst was the bipyridyl derivative **Fe3**, producing an increase of selectivity to CO (entry 12, Table 3) but the total turnover decreased with respect to the phenanthroline-based system **Fe1b**. The cobalt complex **Co3** with the same bipyridyl ligand produced a TON of hydrogen 115 (94 % of selectivity) (entry 13, Table 3).

To analyse the participation of the non-innocent redox ligands in the catalytic activity, the previously reported Zn(**1**)Cl_2 complex [49], containing a non-redox active metal Zn(II) was used as catalyst under the same conditions and produced low amount of CO (TON_{CO} 0.9) and H_2 (TON_{H2} 4, entry 14, Table 3) what indicates that the redox-active ligand requires the presence of an also redox-active metal for the catalysis to take place.

The addition of mixtures BIH/TEOA have been reported to lead to systems more active than when only BIH or TEOA are used separately; BIH acts as a quencher for the excited state of $[Ru(bpy)_3]^{2+}$ and TEOA as a proton acceptor for $BIH^{+\cdot}$ [26,63,64]. The effect of adding different concentrations of BIH to mixtures of TEOA/MeCN was analysed (Table 4). In the absence of Fe complex, the BIH/TEOA/MeCN/**PS1** system produced a mixture of CO/H_2 27/73 with a modest TON (TON_{CO} 14, entry 1, Table 4). Using BIH in MeCN without the addition of TEOA, the system produced only < 1 of TON_{CO} (entry 2, Table 4) which might be attributed to the reversible electron transfer process between the

Table 4
Effect of BIH in the photoreduction of CO_2[a].

Run	Catalyst	BIH (M)	CO (μmol)	TON_{CO} (%Sel.)	H_2 (μmol)	TON_{H2} (%Sel.)	TOF_{CO} (h^{-1})[b]
1	–	0.1	21.0	14 (27)	57.8	38 (73)	–
2[c]	Fe1b	0.1	0.9	1 (17)	4.2	3 (83)	0.1
3	Fe1b	0.1	50.8	34 (32)	108.4	72 (68)	6
4	Fe1b	0.15	242.1	162 (68)	112.6	75 (32)	29
5	Fe1b	0.3	92.9	62 (53)	82.8	55 (47)	19
6	Fe3	0.1	63.7	42 (75)	26.7	18 (25)	12
7[d]	Fe1b	0.3	26.4	17 (14)	164.9	110 (86)	4

[a] Reaction conditions: Catalyst 0.4 mM; TEOA/MeCN: 1/5 v/v; PS = $[Ru(bpy)_3]PF_6]_2$ (1.66 mM), time 24 h. Light source: blue LED (l = 456, 467 nm). TON = turn over number calculated as mols of product/mol catalyst. [b] TOF = averaged turn over frequency after 4 h calculated as mols of CO/mol catalyts·h. [c] No TEOA. [d] After 20 min bubbling CO_2 into final solution of run 5, time = 4 h.

reduced PS^- and the $BIH^{\bullet+}$, in the absence of the base to pick up the proton from the BIH* [64]. However, coupling BIH with TEOA in the presence of the iron complex **Fe1b,** the photoirradiation led to an increase in the generation of CO (entries 3–5, Table 4) reaching a maximum at a concentration of BIH of 0.15 M (up to TON 166 and 68 % selectivity, entry 4, Table 4). The bipyridine complex **Fe3** produced slightly better conversion and selectivity under the same conditions (entry 6, Table 4).

To determine the stability of the catalytic system, in run 5 (Table 4), after the 24 irradiation, CO_2 was bubbled into the final solution again for 20 min and placed under irradiation. After 4 h the gas phase contained a mixture 14/86 of CO/H_2 (TON_{CO} 17, entry 7, Table 4) which is indicative that the decomposition of the catalyst took place under these conditions. The evolution of the TON along the time for experiment 4 using the **Fe1b** catalyst (Table 4) shows that the system activity increased during the first 24 h but a decrease of activity is observed at 48 h, indicative of decomposition (Fig. 2).

Comparing the results obtained with these systems with some selected examples based on Fe-complexes (Table 5) one can conclude that **Fe1b**-based systems are more active than a simple Fe(II) salt (entry 1, Table 5) [27]. Also, molecular porphyrin-based systems (**Fe4**-**Fe6**, entries 2–4, Table 5) [24,65] show TON values lower than **Fe1b** although these systems are more selective in CO, and the porphyrins act as catalysts and also as PS. For the phenanthroline-based complex **Fe7,** the TON and the selectivity (273 in 12 h and 78 % selectivity in CO, entry 5, Table 5) are slightly higher than the ones obtained with **Fe1b** (166 in 24 h and 68 % selectivity in CO, entry 8, Table 5) although **Fe7** uses a PS containing a rather sophisticated N_2P_2-ligand.[63] Fe-quaterpyridine and quiquepyridine based systems (**Fe8** and **Fe9**) developed by Robert and co-workers are by far the most active mononuclear molecular systems in this area (entries 6–7, Table 5) [26, 27].

3.4. Cyclic voltammetry and computational studies

To identify the species formed under electron transfer conditions for the active complex **Fe1b** the cyclic voltammograms (CVs) were recorded under inert and carbon dioxide atmosphere. Complex **Fe1b** in acetonitrile (MeCN, 0.02 mM) with tetrabutylammoniun hexafluorophosphate NBu_4PF_6 (0.1 M) as electrolyte using ferrocene as external standard (Fc^+/Fc) under nitrogen atmosphere, shows three quasi-reversible reduction processes at −1.01 V, −1.94 V and −2.12 V (black trace, Fig. 3a), which are slightly shifted from the values of the reference zinc complex **Zn1** (−1.20, −1.90, −2.08 V, Figure S3, Table S5). Since Zn(II) is not participating on the electron transfer processes, these values may indicate a participation of the ligand in the electro-reduction processes as reported for a Fe(II)-bipyridine-diimine complex [37] and were accordingly assigned to the three reductions $\mathbf{1}/\mathbf{1}^-$, $\mathbf{1}^-/\mathbf{1}^{2-}$ and $\mathbf{1}^{2-}/\mathbf{1}^{3-}$ but the $Fe^{II/I}$ reduction cannot be excluded. When CO_2 was bubbled to the solution of **Fe1b** in acetonitrile, an increase in current intensity and a shift of the peaks was observed (−1.11, −1.76 and −1.98 V) (red trace in Fig. 3).

To confirm these hypotheses computational calculations were run on 1- 2- and 3-electron reduced species of complex **Fe1b**. We considered the structure of the most stable isomer, 6-coordinated with *endo-trans/endo-trans* disposition of **1** and with one and two OTf^- ligands substituted by MeCN solvent molecules. In the case of the complex with two MeCN ligands, the geometry optimization of the 1-electron reduced species showed some low energy structures where one of the N atoms of the phenanthroline ligand tended to dissociate. For this reason, 5-coordinated species where also investigated in this case, although finally the results indicated that these species were not the most stable ones. Different spin multiplicities were taken into account for all species and their minimum energy geometries obtained. The whole set of numerical results are collected in Table S3 of Supplementary information. At all levels of reduction, the most stable systems corresponded to the complexes where the two OTf^- ligands were substituted by MeCN solvent molecules (relative energies shown in Table 6). For this reason, these complexes were the ones analysed in more detail.

As seen in Table 6, the most stable species for the 3 levels of reduction are always the highest spin isomers of the $[Fe(\mathbf{1})(MeCN)_2]^q$ complexes (q = 1, 0, −1 for the 1-, 2- and 3-electron reduced species respectively).

To elucidate the allocation of the electrons incorporated in the reduction process (on the metal centre or on the ligand), structures, calculated Mulliken charges and spin densities were analysed. These results are shown in Table 7 for the most stable isomers of each

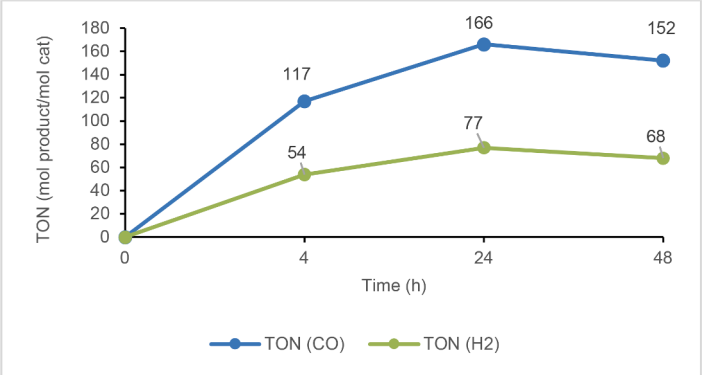

Fig. 2. TON obtained in the photoreduction of CO_2 using **Fe1b** catalyst 0.4 mM; TEOA/MeCN: 1/5 v/v (0.62/3.10 mL); **PS** = $[Ru(bpy)_3]PF_6]$ (1.66 mM). Light source: blue LED (l = 457, 467 nm) Photosensitizers (PS) used in photoreduction of CO_2. (For interpretation of the references to color in this figure legend, the reader is referred to the web version of this article.)

Table 5
Comparison with selected Fe(II)-based catalytic systems for the photoreduction of CO_2.

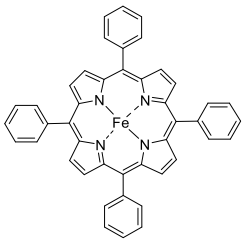

Fe4

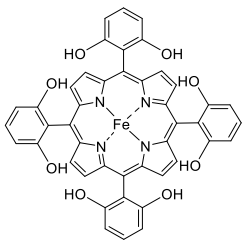

Fe5

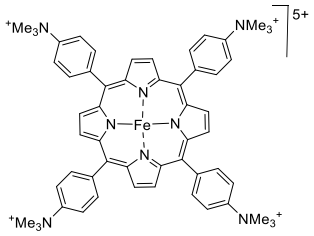

Fe6

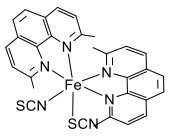

Fe7

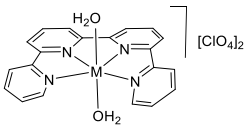

Fe8

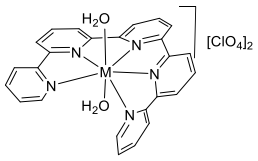

Fe9

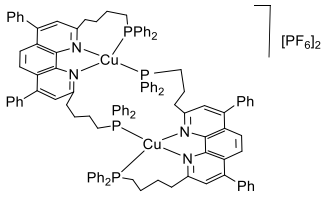

PS2

Entry	Cat	Conditions: PS/SD/Solvent/ λ nm/ t(h)	Main product (TON)[b]	Sel. CO (%)	Other products%,(product)	Ref
1	Fe $(ClO_4)_2$	PS1/MeCN (1:5 v/v)/BIH/LED λ 460 nm/68 h	CO (82)	85	H_2 (TON: 15)	[27]
2	Fe4	-/TEA (0.36 M)/MeCN/Xe-lamp/10h	CO (17)	8 (1 h)	H_2 (TON 37)	[24]
3	Fe5	-/TEA (0.36 M)/MeCN/Xe-lamp/10h	CO (28)	93 (1 h)	H_2 (TON 10)	[24]
4	Fe6	-/BIH (20 mM)/MeCN/Solar simulator λ > 420/47h	CO (63)	100	–	[65]
5	Fe7	PS2/TEOA/MeCN (1:5 v/v)/BIH/250 W Hg λ 436 nm/12 h	CO (273)	78	H_2 (TON: 75)	[63]
6	Fe8	PS1/TEOA/MeCN (1:5 v/v)/BIH/LED λ 460 nm/0.75 h	CO (3844)	85	$HCOO^-$(TON 534, 12 %) H_2 (TON 118, 3 %)	[26]
7	Fe9	PS1/MeCN-H_2O (1:1 v/v)/BIH/LED λ 460 nm/68 h	CO (14,095)	98	–	[27]
8	Fe1b	PS1/TEOA/MeCN (1:5 v/v)/LED λ 456, nm/24 h	CO (166)	68	H_2 (TON: 77)	This work

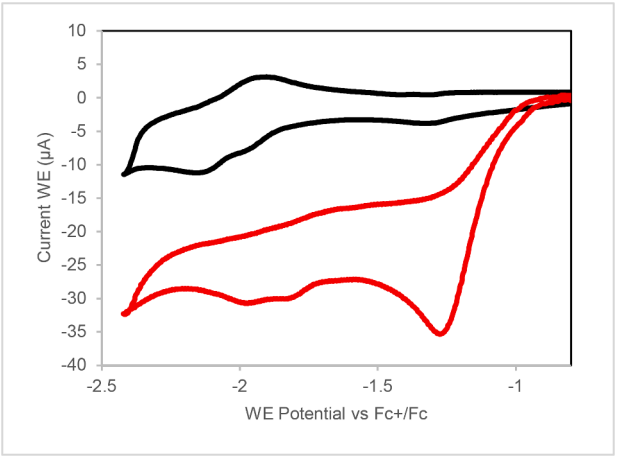

Fig. 3. CV of Fe1b under nitrogen (black) and under CO_2 atmosphere (red) in MeCN (0.02 mM) with NBu_4PF_6 (0.1 M) at scan rate 50 mV·s-1. Working electrode: 3 mm diameter glassy carbon. Counter electrode: Pt wire. Reference electrode: Ag/AgCl (3 M KCl). Values referenced to Fc^+/Fc. (For interpretation of the references to color in this figure legend, the reader is referred to the web version of this article.)

reduction level (the results for all spin symmetry species (Table S4) and the analysis of these results can be found in the Supplementary Information).

It is convenient to point out that Mulliken charges are calculated considering the electron density located in a fixed area of space around each atom. In the case of the central Fe atom, the electrons donated by

Table 6
Relative free energies (in kcal mol^{-1}) of the 1-, 2- and 3-electron reduced most stable species of different multiplicities of the complex **Fe1b** complex, that in all cases correspond to the system with 2 MeCN ligands. Non-reduced complex included for comparison purposes.

Species	n. e^- reduced	Multiplicity	ΔG (kcal/mol)
$[Fe(1)(MeCN)_2]^{+2}$	0	5	0.0
$[Fe(1)(MeCN)_2]^{+1}$	1	4	−76.4
		6	−86.1
$[Fe(1)(MeCN)_2]^0$	2	3	−150.6
		5	−157.5
		7	−161.4
$[Fe(1)(MeCN)_2]^{-1}$	3	3	−217.3
		5	−224.0

the surrounding ligands are included in this area, so the Mulliken charge cannot be interpreted as the oxidation state of the metal, but used only to analyse trends.

The non-reduced species (spin multiplicity $M = 5$), shows the spin density mainly on the central Fe atom, what indicates that the unpaired spin-parallel electrons are on the d orbitals of this atom, as expected.

When 1 or 2 electrons are transferred to the complex, neither the charge nor the spin density on Fe change significantly. This, together with the spin density distribution plot, show that the incorporated electrons are allocated in the imine groups of the phenanthroline ligand, spin-parallel to the unpaired electrons of Fe. Similar results have been found for other bis(imino)pyridine[66–68] and bipyridine-diimine [37] metal complexes, where the ligand-based reduction is mainly located in the imine moieties.

In the 3-electron reduced species, two of the transferred electrons are

Table 7
Spin density distribution (blue and green indicate positive or negative spin), Mulliken charge and spin density over the central Fe atom and distances between the metal centre and the N atoms of the two acetonitrile ligands for the most stable species of non-reduced and 1-, 2- and 3-electron reduced $[Fe(\mathbf{1})(MeCN)_2]^q$ complexes.

	Non-reduced $[Fe(\mathbf{1})(MeCN)_2]^{+2}$	1-electron reduced $[Fe(\mathbf{1})(MeCN)_2]^{+1}$	2-electron reduced $[Fe(\mathbf{1})(MeCN)_2]^{0}$	3-electron reduced $[Fe(\mathbf{1})(MeCN)_2]^{-1}$
Multiplicity	Quintuplet	Sextuplet	Heptaplex	Sextuplet
ΔG (kcal mol^{-1})	0.00	−86.1	−161.4	−224.0
Spin density distribution	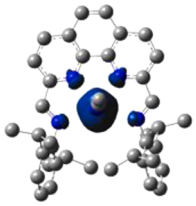	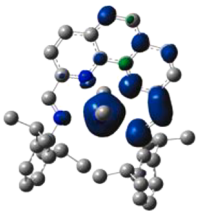	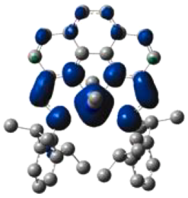	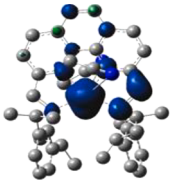
Q_{Fe}	−5.38	−5.28	−5.40	−0.48
Spin density	4.39	4.33	4.39	3.64
$d_{Fe\text{-}N(MeCN)}$ (Å)	2.15; 2.16	2.13; 2.14	2.29; 2.29	4.38; 4.41

located on one of the imine moieties, giving place to null spin density there, while the third electron is located in the other imine group, coupled parallel to the unpaired electros of the Fe centre. The increased electron density in the imine moieties must enhance the donor character of their N atoms, what could be the reason to induce a dissociation of the acetonitrile ligands, that appear at distances around 4.4 Å from the metal centre. This could enhance the activity of the complex as catalyst due to a better disposition to coordinate the substrate. As a subsequent result of the remote position of the MeCN ligands, the accounted charge and spin density around Fe centre is much lower than in the other complexes.

As a whole, these computational results confirm the hypothesis proposed based on experimental evidences of the location of the transferred electrons in the ligand instead on in the metal centre.

Mechanism proposal

Based on previously reported data, the catalytic experiments and the computational calculations performed herein, a mechanism is proposed for the CO_2 reduction to CO by a photocatalytic system formed by **Fe1b** as catalyst and **PS1** as photosensitizer, in the presence of BIH/TEOA in a CO_2 saturated MeCN solution under visible irradiation (Scheme 2). The catalyst precursor **Fe1b** undergoes substitution of the OTf$^-$ ligands by the acetonitrile solvent. This substitution may be favored by catalyst with ligand **1** that generates more steric repulsions than ligand **2** giving place to a more active system. In fact, the lower molar conductivity values of **Fe2** than of **Fe1b** in acetonitrile indicate partial dissociation of the ionic OTf$^-$. The solvated species $[Fe(\mathbf{1})(S)_2]^{2+}$ (S = MeCN) will accept one electron which will be provided through the process of light excitement of **PS1**. Thus, according to the literature, **PS1** is excited by the irradiation of incident light, to generate the excited state **PS1*** (i, Scheme 2) which is reductively quenched by the powerful reductant BIH to give **PS1**$^-$ and $BIH^{\bullet+}$ [69]. The reduced **PS1**$^-$ is a strong reductant, that provides the first electron to the catalyst, which according to the cyclic voltammetry and computational studies is located in the ligand framework forming the $[Fe(\mathbf{1}^{\bullet-})(S)_2]^{+}$ species.

Given the position of the catalytic peak that increases in the CV when CO_2 is added to the system, corresponding to the 1-electron transfer, it can be supposed that is the one-electron reduced species $[Fe(\mathbf{1}^{\bullet-})(S)_2]^{+}$ the one that coordinates CO_2, which after the second electron uptake will form $[Fe(\mathbf{1})(S)CO_2]^{0}$ (ii, Scheme 2). The steric effects of the framework catalyst formed by the tetradentate ligand may affect the substitution steps of the proposed catalytic cycle. That is the OTf$^-$ substitution by the solvent or the solvent substitution by CO_2. The higher the steric effect, the faster de substitution step will be. Regarding the flexibility of the aromatic skeleton, it may affect the stability and coordination number of the intermediates influencing the activity and selectivity.

The second electron may be subsequently provided by radical $BI^{\bullet}$, formed according to literature by deprotonation of $BIH^{\bullet+}$ in the presence of TEOA (iii, Scheme 2) [70], giving place to the species $[Fe(\mathbf{1})(S)CO_2]^{0}$ (ii, Scheme 2). Two additional H^+ are needed at this stage to break

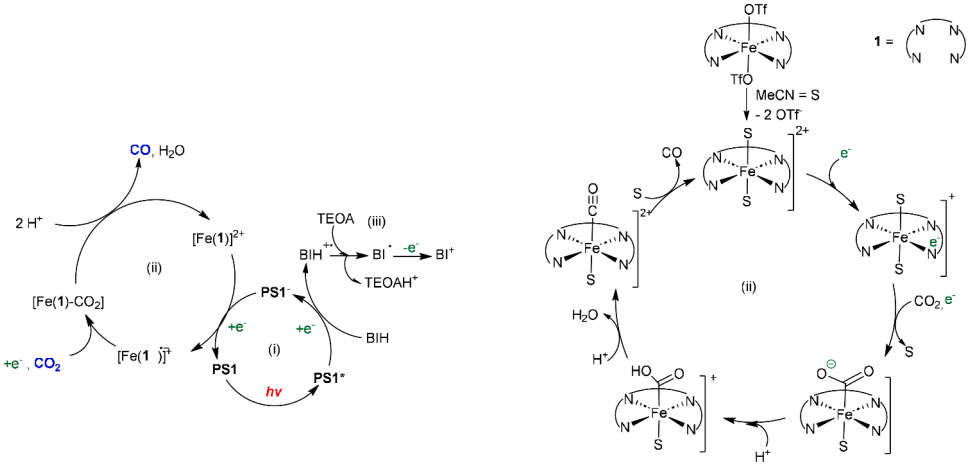

Scheme 2. Proposed mechanism for CO_2 photoreduction towards CO with **Fe1b** catalyst using **PS1** in BIH/TEOA/CH_3CN system. (i) Photosensitiser cycle and (ii) catalyst proposed species for the catalytic cycle.

the CO_2 bond, release CO, and regenerate the catalyst, as illustrated in Scheme 2 (ii).

5. Conclusions

Iron(II), cobalt(II) and nickel(II) complexes with non-innocent redox N4-donor ligands with phenanthroline and bipyridine skeleton have been prepared and applied to the photoreduction of CO_2 in presence of a photosensitizer and sacrificial electron donor. The more stable structures have been proposed based on computational calculations. The Fe (II) catalytic systems provide mixtures of CO/H_2 reaching a maximum selectivity in CO of 68 % with a modest TON_{CO} of 166 while Co(II) and Ni(II) led to the formation of H_2 as a major product. Cyclic voltammetry studies show that the electron uptakes are centered in the N4-donor ligands. Computational calculations allow to propose the most stable location of the electrons. The steric effect of the ligands influence the activity of the catalyst modifiyng the substitution reactions involved in the catalytic cycle.

CRediT authorship contribution statement

Nassima El Aouni: Investigation. **Ali Aghmiz:** Supervision. **Mar Reguero:** Writing – review & editing, Writing – original draft, Supervision, Investigation, Conceptualization. **Anna M. Masdeu-Bultó:** Writing – review & editing, Writing – original draft, Supervision, Investigation, Funding acquisition, Conceptualization.

Declaration of competing interest

The authors declare that they have no known competing financial interests or personal relationships that could have appeared to influence the work reported in this paper.

Data availability

Data will be made available on request.

Acknowledgements

The authors are thankful to the Spanish Ministerio de Ciencia e Innovación and AEI/FEDER UE (PID2019-104427RB-100 and PID2020-113187GB-I00), the Generalitat de Catalunya Departament de Recerca i Universitats (AGAUR 2021 SGR 00163, 2021 SGR 00110 and N. El Aouni grant 2019 FI-B 00784) and Xarxa d'R+D+I en Química Computacional (XRQTC) and The Centre National pour la Recherche Scientifique et Technique (CNRST / Maroc) (Programme PBER N: 9UAE2019).

Supplementary materials

Supplementary material associated with this article can be found, in the online version, at doi:10.1016/j.mcat.2024.114392.

References

[1] M. Pathak, R. Slade, P.R. Shukla, J. Skea, R. Pichs-Madruga, D. Ürge-Vorsatz, Climate change 2022: mitigation of climate change. Contribution of Working Group III to the Sixth Assessment Report of the Intergovernmental Panel on Climate Change, Technical Summary, Cambridge, 2022, https://doi.org/10.1017/9781009157926.002.
[2] IPCC, Climate Change 2013. The Physical Science Basis, 2013.
[3] N.Mac Dowell, P.S. Fennell, N. Shah, G.C. Maitland, The role of CO2 capture and utilization in mitigating climate change, Nat. Clim. Chang. 7 (2017) 243–249, https://doi.org/10.1038/nclimate3231.
[4] T.P. Senftle, E.A. Carter, The holy grail: chemistry enabling an economically viable CO2 capture, utilization, and storage strategy, Acc. Chem. Res. 50 (2017) 472–475, https://doi.org/10.1021/acs.accounts.6b00479.
[5] Q. Liu, L. Wu, R. Jackstell, M. Beller, Using carbon dioxide as a building block in organic synthesis, Nat. Commun. 6 (2015) 5933, https://doi.org/10.1038/ncomms6933.
[6] P.R. Yaashikaa, S. Swetha, B. Reshma, A comprehensive review on different approaches for CO 2 utilization and conversion pathways, Chem. Eng. Sci. (2021), https://doi.org/10.1016/j.ces.2021.116515.
[7] M. Aresta, A. Dibenedetto, A. Angelini, The changing paradigm in CO2 utilization, J. CO2 Util. 3-4 (2013) 65–73, https://doi.org/10.1016/j.jcou.2013.08.001.
[8] M. Robert, Running the clock: CO2 catalysis in the age of anthropocene, ACS Energy Lett. 1 (2016) 281–282, https://doi.org/10.1021/acsenergylett.6b00159.
[9] C. George, Carbon Monoxide, Kirk-Othmer Encyclopedia of Chemical Technology, John Wiley & Sons, Inc., Hoboken, NJ, USA, 2001, https://doi.org/10.1002/0471238961.0301180216090518.a02.pub2.
[10] J.-Y. Li, L. Yuan, S.-H. Li, Z.-R. Tang, Y.-J. Xu, One-dimensional copper-based heterostructures toward photo-driven reduction of CO $_2$ to sustainable fuels and feedstocks, J. Mater. Chem. A 7 (2019) 8676–8689, https://doi.org/10.1039/C8TA12427B.
[11] L.-H. Gao, W.-Y. Xiao, M.-Y. Qi, J.-Y. Li, C.-L. Tan, Z.-R. Tang, Photoredox-catalyzed coupling of CO2 reduction and amines oxidation by Cu doped CdS quantum dots, Mol. Catal. 554 (2024) 113858, https://doi.org/10.1016/j.mcat.2024.113858.
[12] M. Qi, Y. Xu, Efficient and direct functionalization of allylic sp^3 C−H bonds with concomitant CO $_2$ reduction, Angew. Chem. 135 (2023) e202311731, https://doi.org/10.1002/ange.202311731.
[13] M.-Y. Qi, Q. Lin, Z.-R. Tang, Y.-J. Xu, Photoredox coupling of benzyl alcohol oxidation with CO2 reduction over CdS/TiO2 heterostructure under visible light irradiation, Appl. Catal. B 307 (2022) 121158, https://doi.org/10.1016/j.apcatb.2022.121158.
[14] F.D. Rossini, R.S. Jessup, Heat and free energy of formation of carbon dioxide, and of the transition between graphite and diamond, J. Res. Natl. Bur. Stand. 21 (1938) 491, https://doi.org/10.6028/jres.021.028.
[15] G.W. Crabtree, N.S. Lewis, Solar energy conversion, Phys. Today 60 (2007) 37–42, https://doi.org/10.1063/1.2718755.
[16] J.L. White, M.F. Baruch, J.E. Pander, Y. Hu, I.C. Fortmeyer, J.E. Park, T. Zhang, K. Liao, J. Gu, Y. Yan, T.W. Shaw, E. Abelev, A.B. Bocarsly, Light-driven heterogeneous reduction of carbon dioxide: photocatalysts and photoelectrodes, Chem. Rev. 115 (2015) 12888–12935, https://doi.org/10.1021/acs.chemrev.5b00370.
[17] R. Kamata, H. Kumagai, Y. Yamazaki, M. Higashi, R. Abe, O. Ishitani, Durable photoelectrochemical CO2reduction with water oxidation using a visible-light driven molecular photocathode, J. Mater. Chem. A 9 (2021) 1517–1529, https://doi.org/10.1039/d0ta07351b.
[18] H. Tian, Molecular catalyst immobilized photocathodes for water/proton and carbon dioxide reduction, ChemSusChem. 8 (2015) 3746–3759, https://doi.org/10.1002/cssc.201500983.
[19] T. Morikawa, S. Sato, K. Sekizawa, T.M. Suzuki, T. Arai, Solar-driven CO $_2$ reduction using a semiconductor/molecule hybrid photosystem: from photocatalysts to a monolithic artificial leaf, Acc. Chem. Res. 55 (2022) 933–943, https://doi.org/10.1021/acs.accounts.1c00564.
[20] H. Kumagai, Y. Tamaki, O. Ishitani, Photocatalytic systems for CO2 reduction: metal-complex photocatalysts and their hybrids with photofunctional solid materials, Acc. Chem. Res. 55 (2022) 978–990, https://doi.org/10.1021/acs.accounts.1c00705.
[21] F. Zaera, Designing sites in heterogeneous catalysis: are we reaching selectivities competitive with those of homogeneous catalysts? Chem. Rev. 122 (2022) 8594–8757, https://doi.org/10.1021/acs.chemrev.1c00905.
[22] E. Boutin, L. Merakeb, B. Ma, B. Boudy, M. Wang, J. Bonin, E. Anxolabéhère-Mallart, M. Robert, Molecular catalysis of CO $_2$ reduction: recent advances and perspectives in electrochemical and light-driven processes with selected Fe, Ni and Co aza macrocyclic and polypyridine complexes, Chem. Soc. Rev. 49 (2020) 5772–5809, https://doi.org/10.1039/D0CS00218F.
[23] J. Bonin, M. Chaussemier, M. Robert, M. Routier, Homogeneous photocatalytic reduction of CO<inf>2</inf>to CO using iron(0) porphyrin catalysts: mechanism and intrinsic limitations, ChemCatChem. 6 (2014) 3200–3207, https://doi.org/10.1002/cctc.201402515.
[24] J. Bonin, M. Robert, M. Routier, Selective and efficient photocatalytic CO $_2$ reduction to CO using visible light and an iron-based homogeneous catalyst, J. Am. Chem. Soc. 136 (2014) 16768–16771, https://doi.org/10.1021/ja510290t.
[25] P.G. Alsabeh, A. Rosas-Hernández, E. Barsch, H. Junge, R. Ludwig, M. Beller, Iron-catalyzed photoreduction of carbon dioxide to synthesis gas, Catal. Sci. Technol. 6 (2016) 3623–3630, https://doi.org/10.1039/c5cy01129a.
[26] Z. Guo, S. Cheng, C. Cometto, E. Anxolabéhère-Mallart, S.-M. Ng, C.-C. Ko, G. Liu, L. Chen, M. Robert, T.-C. Lau, Highly efficient and selective photocatalytic CO 2 reduction by iron and cobalt quaterpyridine complexes, J. Am. Chem. Soc. 138 (2016) 9413–9416, https://doi.org/10.1021/jacs.6b06002.
[27] Y. Qin, L. Chen, G. Chen, Z. Guo, L. Wang, H. Fan, M. Robert, T.C. Lau, A highly active and robust iron quinquepyridine complex for photocatalytic CO2reduction in aqueous acetonitrile solution, Chem. Commun. 56 (2020) 6249–6252, https://doi.org/10.1039/d0cc01930e.
[28] F. Liu, J. Bi, Y. Sun, S. Luo, P. Kang, Cobalt complex with redox-active imino bipyridyl ligand for electrocatalytic reduction of carbon dioxide to formate, ChemSusChem. 11 (2018) 1656–1663, https://doi.org/10.1002/cssc.201800136.
[29] J.S. Derrick, M. Loipersberger, R. Chatterjee, D.A. Iovan, P.T. Smith, K. Chakarawet, J. Yano, J.R. Long, M. Head-Gordon, C.J. Chang, Metal-ligand cooperativity via exchange coupling promotes iron- catalyzed electrochemical

co2reduction at low overpotentials, J. Am. Chem. Soc. 142 (2020) 20489–20501, https://doi.org/10.1021/JACS.0C10664/SUPPL_FILE/JA0C10664_SI_001.CIF.
[30] L. Gracia, E. Barani, J. Braun, A.B. Carter, O. Fuhr, A.K. Powell, K. Fink, C. Bizzarri, Photocatalytic reduction of CO $_2$ by highly efficient homogeneous Fe ^{II} catalyst based on 2,6-Bis(1',2',3'-triazolyl-methyl)pyridine. Comparison with analogues, ChemCatChem. 14 (2022) e202201163, https://doi.org/10.1002/cctc.202201163.
[31] P. De La Torre, J.S. Derrick, A. Snider, P.T. Smith, M. Loipersberger, M. Head-Gordon, C.J. Chang, Exchange coupling determines metal-dependent efficiency for iron-and cobalt-catalyzed photochemical CO2 reduction, ACS Catal. 12 (2022) 8484–8493, https://doi.org/10.1021/ACSCATAL.2C02072/SUPPL_FILE/CS2C02072_SI_001.CIF.
[32] F. Droghetti, A. Amati, F. Pascale, A. Crochet, M. Pastore, A. Ruggi, M. Natali, Catalytic CO2 reduction with heptacoordinated polypyridine complexes: switching the selectivity via metal replacement, ChemSusChem. (2023), https://doi.org/10.1002/cssc.202300737.
[33] S. Matsuoka, K. Yamamoto, C. Pac, S. Yanagida, Enhanced p -terphenyl-catalyzed photoreduction of CO 2 to CO through the mediation of Co(III)–cyclam complex, Chem. Lett. 20 (1991) 2099–2100, https://doi.org/10.1246/cl.1991.2099.
[34] S. Matsuoka, K. Yamamoto, T. Ogata, M. Kusaba, N. Nakashima, S. Yanagida, E. Fujita, Efficient and selective electron mediation of cobalt complexes with cyclam and related macrocycles in the p-terphenyl-catalyzed photoreduction of CO2, J. Am. Chem. Soc. 115 (1993) 601–609, https://doi.org/10.1021/ja00055a032.
[35] J. Hawecker, J.-M. Lehn, R. Ziessel, Efficient photochemical reduction of CO $_2$ to CO by visible light irradiation of systems containing *Re*(bipy)(CO) $_3$ X or Ru(bipy) $_3$ $^{2+}$ –Co $^{2+}$ combinations as homogeneous catalysts, J. Chem. Soc. Chem. Commun. (1983) 536–538, https://doi.org/10.1039/C39830000536.
[36] J. Hawecker, J.-M Lehn, R. Ziessel, Photochemical and electrochemical reduction of carbon dioxide to carbon monoxide mediated by (2,2′-Bipyridine) tricarbonylchlororhenium(I) and related complexes as homogeneous catalysts, Helv. Chim. Acta 69 (1986) 1990–2012, https://doi.org/10.1002/hlca.19860690824.
[37] R. Thenarukandiyil, E. Paenurk, A. Wong, N. Fridman, A. Karton, R. Carmieli, G. Ménard, R. Gershoni-Poranne, G. de Ruiter, Extensive redox non-innocence in iron bipyridine-diimine complexes: a combined spectroscopic and computational study, Inorg. Chem. 60 (2021) 18296–18306, https://doi.org/10.1021/acs.inorgchem.1c02925.
[38] V. Lyaskovskyy, B. De Bruin, Redox non-innocent ligands: versatile new tools to control catalytic reactions, ACS Catal. 2 (2012) 270–279, https://doi.org/10.1021/cs200660v.
[39] X. Su, K.M. Mccardle, J.A. Panetier, J.W. Jurss, R. Li, Electrocatalytic CO2 reduction with nickel complexes supported by tunable bipyridyl-N-heterocyclic carbene donors: understanding redox-active macrocycles, Chem. Commun. 54 (2018) 3351–3354, https://doi.org/10.1039/C8CC00266E.
[40] X. Su, K.M. McCardle, L. Chen, J.A. Panetier, J.W. Jurss, Robust and selective cobalt catalysts bearing redox-active bipyridyl- N-heterocyclic carbene frameworks for electrochemical CO2 reduction in aqueous solutions, ACS Catal. 9 (2019) 7398–7408, https://doi.org/10.1021/ACSCATAL.9B00708/ASSET/IMAGES/LARGE/CS-2019-007086_0008.JPEG.
[41] Y. Wu, J. Jiang, Z. Weng, M. Wang, D.L.J. Broere, Y. Zhong, G.W. Brudvig, Z. Feng, H. Wang, Electroreduction of CO2 catalyzed by a heterogenized Zn-porphyrin complex with a redox-innocent metal center, ACS Cent. Sci. 3 (2017) 847–852, https://doi.org/10.1021/acscentsci.7b00160.
[42] M.J. Frisch, G.W. Trucks, H.B. Schlegel, G.E. Scuseria, M.A. Robb, J.R. Cheeseman, G. Scalmani, V. Barone, G.A. Petersson, H. Nakatsuji, X. Li, M. Caricato, A. V. Marenich, J. Bloino, B.G. Janesko, R. Gomperts, B. Mennucci, H.P. Hratchian, J. V. Ortiz, A.F. Izmaylov, J.L. Sonnenberg, D. Williams-Young, F. Ding, F. Lipparini, F. Egidi, J. Goings, B. Peng, A. Petrone, T.D. Ranasinghe, V.G. Zakrzewski, J. Gao, N. Rega, G. Zheng, W. Liang, M. Hada, M. Ehara, K. Toyota, R. Fukuda, J. Hasegawa, M. Ishida, T. Nakajima, Y. Honda, O. Kitao, H. Nakai, T. Vreven, K. Throssell Jr., J.A. Montgomery, J.E. Peralta, F. Ogliaro, M.J. Bearpark, J. J. Heyd, E.N. Brothers, K.N. Kudin, V.N. Staroverov, T.A. Keith, R. Kobayashi, J. Normand, K. Raghavachari, A.P. Rendell, J.C. Burant, S.S. Iyengar, J. Tomasi, M. Cossi, J.M. Millam, M. Klene, C. Adamo, R. Cammi, J.W. Ochterski, R.L. Martin, K. Morokuma, O. Farkas, J.B. Foresman, D.J. Fox, Gaussian 16 Rev. C.01, 2016.
[43] J. Tomasi, B. Mennucci, R. Cammi, Quantum mechanical continuum solvation models, Chem. Rev. 105 (2005) 2999–3093, https://doi.org/10.1021/cr9904009.
[44] S. Céspedes Paredes, M. Reguero, Personal Communication, 2017.
[45] Y. Kuramochi, M. Kamiya, H. Ishida, Photocatalytic CO $_2$ reduction in *N, N* -dimethylacetamide/water as an alternative solvent system, Inorg. Chem. 53 (2014) 3326–3332, https://doi.org/10.1021/ic500050q.
[46] Y. Kuramochi, M. Sekine, K. Kitamura, Y. Maegawa, Y. Goto, S. Shirai, S. Inagaki, H. Ishida, Photocatalytic CO $_2$ reduction by Periodic Mesoporous Organosilica (PMO) containing two different ruthenium complexes as photosensitizing and catalytic sites, Chemistry 23 (2017) 10301–10309, https://doi.org/10.1002/chem.201701466.
[47] X.-B. Lu, H. Wang, R. He, Aluminum phthalocyanine complex covalently bonded to MCM-41 silica as heterogeneous catalyst for the synthesis of cyclic carbonates, J. Mol. Catal. a Chem. 186 (2002) 33–42, https://doi.org/10.1016/S1381-1169(02)00181-4.
[48] G.A. Griffith, M.J. Al-Khatib, K. Patel, K. Singh, G.A. Solan, Solid and solution state flexibility of sterically congested bis(imino)bipyridine complexes of zinc(II) and nickel(II), Dalton. Trans. 2 (2009) 185–196, https://doi.org/10.1039/B811309B.
[49] N. El Aouni, C. López Redondo, M. Bin Yeamin, A. Aghmiz, M. Reguero, A. M. Masdeu-Bultó, Influence of structural properties of zinc complexes with N4-donor ligands on the catalyzed cycloaddition of CO2 to epoxides into cyclic carbonates, Mol. Catal. 538 (2023) 112992, https://doi.org/10.1016/j.mcat.2023.112992.
[50] W.J. Geary, The use of conductivity measurements in organic solvents for the characterisation of coordination compounds, Coord. Chem. Rev. 7 (1971) 81–122.
[51] G.J.P. Britovsek, S.P.D. Baugh, O. Hoarau, V.C. Gibson, D.F. Wass, A.J.P. White, D. J. Williams, The role of bulky substituents in the polymerization of ethylene using late transition metal catalysts: a comparative study of nickel and iron catalyst systems, Inorgan. Chim. Acta 345 (2003) 279–291, https://doi.org/10.1016/S0020-1693(02)01293-8.
[52] L. Wang, W.H. Sun, L. Han, H. Yang, Y. Hu, X. Jin, Late transition metal complexes bearing 2,9-bis(imino)-1,10-phenanthrolinyl ligands: synthesis, characterization and their ethylene activity, J. Organomet. Chem. 658 (2002) 62–70, https://doi.org/10.1016/S0022-328X(02)01623-6.
[53] A. Begum, O. Seewald, U. Flörke, G. Henkel, Structural and NMR spectroscopic investigations of Cu(I), Cu ^{II}, Ni ^{II}, Zn ^{II} and Fe ^{II} complexes of 2, 9-di-(Benzothiazolino)-1,10-phenanthroline, ChemistrySelect. 1 (2016) 2257–2264, https://doi.org/10.1002/slct.201600505.
[54] S. Ameerunisha, J. Schneider, T. Meyer, G. Henkel, P.S. Zacharias, E. Bill, Synthesis and structural characterisation of Fe(ii) and Cu(i) complexes of a new tetrafunctional N-donor ligand with dodecahedral or tetrahedral binding domains, Chem. Commun. (2000) 2155–2156, https://doi.org/10.1039/b005671p.
[55] F. Vega, M. Cano, S. Camino, L.M.G. Fernández, E. Portillo, B. Navarrete, Solvents for carbon dioxide capture. Carbon Dioxide Chemistry, Capture and Oil Recovery, InTech, 2018, https://doi.org/10.5772/intechopen.71443.
[56] K. Zhang, Q. Gao, C. Xu, D. Zhao, Q. Zhu, Z. Zhu, J. Wang, C. Liu, H. Yu, C. Sun, X. Liu, Y. Xuan, Current dilemma in photocatalytic CO2 reduction: real solar fuel production or false positive outcomings? Carbon Neutral. 1 (1) (2022) 1–16, https://doi.org/10.1007/S43979-022-00011-X.
[57] M. Zhang, M. El-Roz, H. Frei, J.L. Mendoza-Cortes, M. Head-Gordon, D.C. Lacy, J. C. Peters, Visible light sensitized CO $_2$ activation by the tetraaza [Co ^{II} N $_4$ H (MeCN)] $^{2+}$ complex investigated by FT-IR spectroscopy and DFT calculations, J. Phys. Chem. C 119 (2015) 4645–4654, https://doi.org/10.1021/jp5127738.
[58] K. Mochizuki, S. Manaka, I. Takeda, T. Kondo, Synthesis and structure of [6,6′-Bi (5,7-dimethyl-l,4,8,11-tetraazacyclotetradecane)]dinickel(II) inflate and its catalytic activity for photochemical CO2 reduction, Inorg. Chem. 35 (1996) 5132–5136, https://doi.org/10.1021/IC960208E.
[59] J.L. Grant, K. Goswami, L.O. Spreer, J.W. Otvos, M. Calvin, Photochemical reduction of carbon dioxide to carbon monoxide in water using a nickel(II) tetra-azamacrocycle complex as catalyst, J. Chem. Soc. Dalton Trans. (1987) 2105, https://doi.org/10.1039/dt9870002105.
[60] P. Kang, C. Cheng, Z. Chen, C.K. Schauer, T.J. Meyer, M. Brookhart, Selective electrocatalytic reduction of CO 2 to formate by water-stable iridium dihydride pincer complexes, J. Am. Chem. Soc. 134 (2012) 5500–5503, https://doi.org/10.1021/ja300543s.
[61] M.R. Bohloul, A. Vatani, S.M. Peyghambarzadeh, Experimental and theoretical study of CO2 solubility in N-methyl-2-pyrrolidone (NMP), Fluid. Phase Equilib. 365 (2014) 106–111, https://doi.org/10.1016/j.fluid.2013.12.019.
[62] K. Ding, F. Zannat, J.C. Morris, W.W. Brennessel, P.L. Holland, Coordination of N-methylpyrrolidone to iron(II), J. Organomet. Chem. 694 (2009) 4204–4208, https://doi.org/10.1016/j.jorganchem.2009.09.005.
[63] H. Takeda, K. Ohashi, A. Sekine, O. Ishitani, Photocatalytic CO2 reduction using Cu (I) photosensitizers with a Fe(II) catalyst, J. Am. Chem. Soc. 138 (2016) 4354–4357, https://doi.org/10.1021/jacs.6b01970.
[64] Y. Tamaki, K. Koike, T. Morimoto, O. Ishitani, Substantial improvement in the efficiency and durability of a photocatalyst for carbon dioxide reduction using a benzoimidazole derivative as an electron donor, J. Catal. 304 (2013) 22–28, https://doi.org/10.1016/j.jcat.2013.04.002.
[65] H. Rao, J. Bonin, M. Robert, Non-sensitized selective photochemical reduction of CO2 to CO under visible light with an iron molecular catalyst, Chem. Commun. 53 (2017) 2830–2833, https://doi.org/10.1039/c6cc09967j.
[66] B. De Bruin, E. Bill, E. Bothe, T. Weyhermüller, K. Wieghardt, Molecular and electronic structures of bis(pyridine-2,6-diimine)metal complexes [ML2](PF6)(n) (n = 0, 1, 2, 3; M = Mn, Fe, Co, Ni, Cu, Zn), Inorg. Chem. 39 (2000) 2936–2947, https://doi.org/10.1021/ic000113j.
[67] S.C. Bart, K. Chłopek, E. Bill, M.W. Bouwkamp, E. Lobkovsky, F. Neese, K. Wieghardt, P.J. Chirik, Electronic structure of bis(imino)pyridine iron dichloride, monochloride, and neutral ligand complexes: a combined structural, spectroscopic, and computational study, J. Am. Chem. Soc. 128 (2006) 13901–13912, https://doi.org/10.1021/JA064557B/SUPPL_FILE/JA064557BSI20060811_084711.PDF.
[68] A.C. Bowman, C. Milsmann, E. Bill, E. Lobkovsky, T. Weyhermüller, K. Wieghardt, P.J. Chirik, Reduced N -alkyl substituted bis(imino)pyridine cobalt complexes: molecular and electronic structures for compounds varying by three oxidation states, Inorg. Chem. 49 (2010) 6110–6123, https://doi.org/10.1021/IC100717W/SUPPL_FILE/IC100717W_SI_001.CIF.
[69] Y. Pellegrin, F. Odobel, Sacrificial electron donor reagents for solar fuel production, Comptes Rendus Chim. 20 (2016) 283–295, https://doi.org/10.1016/j.crci.2015.11.026.
[70] L. Gimeno, C. Queffelec, E. Blart, Y. Pellegrin, Copper(I) Bis(diimine) complexes with high photooxidation power: reductive quenching of the excited state with a benzimidazoline sacrificial donor, ACS Omega 7 (2022) 13112–13119, https://doi.org/10.1021/acsomega.2c00531.